A Family of Polynuclear Cobalt and Nickel Complexes Stabilised by 2-Pyridonate and Carboxylate Ligands

Cristiano Benelli,[b] Alexander J. Blake,[a] Euan K. Brechin,[a] Simon J. Coles,[c] Alasdair Graham,[a] Steven G. Harris,[a] Stephanie Meier,[a] Andrew Parkin,[a] Simon Parsons,[a] Annela M. Seddon,[a] and Richard E. P. Winpenny*[a]

Abstract: The synthesis and structural characterisation of a series of cobalt and nickel cages are reported. Eight of these structures contain a $[M_{10}(\mu_3\text{-}OH)_6(\eta^2,\mu_3\text{-}xhp)_6(\eta^2,\mu_2\text{-}O_2CR)_6]^{2+}$ core (where M = Co or Ni; xhp = 6-chloro- or 6-methyl-2-pyridonate; R = Me, Ph, $CHMe_2$, CH_2Cl, $CHPh_2$ or CMe_3), where the ten metal atoms describe a centred-tricapped-trigonal prism (ttp). The cage contains six hydroxide ligands around the central metal, and the exterior is coated with pyridonate and carboxylate ligands. For four of the cages additional metal centres are found attached to the upper and/or lower triangular faces of the trigonal prism, generating dodeca- and undecanuclear cages. Three further cages are reported that contain a metal core based on an incomplete centred-tetraicosahedron. These cages involve trimethylacetate as a ligand in company with either 6-methyl-2-pyridonate or 6-chloro-2-pyridonate. Comparison of these latter structures with the trigonal prisms reveal that they can be described as a pentacapped-trigonal prism missing one edge. Magnetic studies of three of the nickel cages with trigonal prismatic cores show spin ground states of $S = 8$, 4 and 2 for Ni_{12}, Ni_{11} and Ni_{10} cages, respectively.

Keywords: cage compounds · cobalt · magnetic properties · N ligands · nickel

Introduction

There is currently a great deal of interest in "single molecule magnets" (SMMs), that is polynuclear cages which display magnetic hysteresis effects which are of a molecular origin.[1–3] This interest has come in part because these cages can exhibit quantum tunnelling of magnetisation,[2] and partly because of the technological implications of molecules which display the characteristics of a magnetic memory. In addition SMMs present a challenge to synthetic and structural chemists because they are difficult to make, often they have unpredictable structures, and because any correlation between structure and magnetic properties is presently unclear.

One approach to the latter problem is to target families of high nuclearity cages, where it may be possible to study series of cages and examine systematically how structure relates to magnetism. Work from the Christou and Hendrickson groups on a series of $\{Mn_{12}\}$ cages has illustrated the possibilities of this approach, as they have shown that the kinetic barrier to re-orientation of magnetisation within these cages can be related to the relative positions of the Jahn–Teller axes of Mn^{III} ions within a structure.[3]

We have been pursuing studies of the later 3d metals,[4] especially cobalt and nickel, as such cages had not previously been studied and initial results indicated that such cages may display unusual magnetic properties.[5, 6] Here we report a study of a simple reaction involving a "blend" of carboxylate and 2-pyridonate ligands, which produces a family of related structures. The reactions develop a 1983 report of a dodecanuclear cobalt cage, $[Co_{12}(OH)_6(mhp)_{12}(O_2CMe)_6]$ (**1**) (mhp = 6-methyl-2-pyridonate).[7] This work, from C. D. Garner's group, appeared fascinating partly due to the beauty of the structure but mainly due to the high nuclearity of the metal array present and the potential it offered for subtle variation. The metal polyhedron present is a centered pentacapped-trigonal prism. We were intrigued that no further studies of this molecule have appeared, and no

[a] Dr. R. E. P. Winpenny, Dr. A. J. Blake, Dr. E. K. Brechin, A. Graham, Dr. S. G. Harris, S. Meier, A. Parkin, Dr. S. Parsons, A. M. Seddon
Department of Chemistry
The University of Edinburgh
West Mains Road
Edinburgh, EH9 3JJ (UK)
Fax: (+44) 131-650-4743
E-mail: repw01@holyrood.ed.ac.uk

[b] Prof. C. Benelli
Department of Chemistry
University of Florence
Via Maragliano 77, 50144 Florence (Italy)

[c] Dr. S. J. Coles
EPSRC Crystallographic Service
Department of Chemistry
University of Southampton
Southampton, SO17 1BJ (UK)

  0947-6539/00/0605-0883 $ 17.50+.50/0

magnetic data have been reported. Compound **1** was synthesised by reaction of anhydrous cobalt acetate with Hmhp at 130 °C, followed by crystallisation from toluene. Here we report reactions where the metal and carboxylate present are varied to generate a series of tricapped-trigonal prisms, and other deltahedra, and the magnetic characterisation of the nickel complexes related to **1**. The structures of four of these complexes have appeared in preliminary communications.[8, 9]

Results

Synthesis

Previously we have explored the reaction of pre-formed metal carboxylates with molten Hmhp or Hchp.[4, 5, 8–10] This reaction produces a paste, which is green or purple depending on whether Ni or Co is the metal present. The carboxylic acid by-product can be boiled out of the paste by heating under reduced pressure. The paste is then extracted with a suitable solvent.

Further studies have led us to believe that pre-forming the metal carboxylate is unnecessary, and that a much easier and more productive series of reactions involves stirring together a metal salt with the sodium salt of both the pyridonate and the carboxylate in a solvent such as MeOH, EtOH or THF. The reaction is stirred for a day, then filtered and evaporated to dryness under reduced pressure. The residue is then dried under vacuum overnight, prior to extraction and crystallisation from either CH_2Cl_2 or MeCN. Undecanuclear species crystallised from CH_2Cl_2, and dodeca- and decanuclear species crystallised from MeCN; however, there seems no rational explanation for this difference.

All these species, including **1**, require the presence of moisture in order to form, with at least six hydroxides present in structures **1**–**9**, and four hydroxides present in structures **10**–**12**. This water presumably arises from the use of hydrated metal salts. If further water is deliberately introduced at the crystallisation stage or earlier in an attempt to improve yields, often intractable powders form which we believe are metal-hydroxide containing materials. The balance between presence of sufficient moisture to allow the cages to form, and too much moisture causing formation of polymeric hydroxide arrays, is a fine one. A crucial factor in developing this chemistry has been the use of moderately large quantities of reactants to allow characterisation of cages which, on occasions, form in yields as low as 10%. Elemental analyses for **2**–**12** are given in Table 1.

Structural studies: Complexes **2**–**9** all contain a core based on a decanuclear centred-tricapped-trigonal prism bridged in a similar manner by hydroxide, carboxylate and pyridonate ligands. Where the nuclearity of the cages differ it is due to the presence or absence of further metals on the trigonal faces of the prism; where the ligands vary it is only in the way in which these upper and lower trigonal faces are ligated. Crystal data and data collection and refinement parameters for compounds **2**–**12** are given in Table 2. Bond lengths and angles for these cages are given in Tables 3 and 4, respectively.

The structure of $[Ni_{12}(OH)_6(mhp)_{12}(O_2CCH_2Cl)_6]$ (**2**) is shown in Figure 1 and the metal polyhedron in Figure 2. The central nickel atom Ni1 is bound to six μ_3-hydroxide ligands which bridge to the nine further metals forming the tricapped trigonal prism. The metal atoms at the vertices of the prism Ni7, Ni8, Ni9, Ni10, Ni11 and Ni12 share one μ_3-OH group with Ni1, while the metal atoms capping the rectangular faces of the prism Ni4, Ni5 and Ni6 share two μ_3-hydroxide ligands with Ni1, forming three M_2O_2 rings.

The exterior of this central tricapped-trigonal prism is bridged by six mhp and six chloroacetate ligands. Each mhp ligand binds to one of the nickel atoms at the vertices of the prism through its N-donor atom, and μ_3-bridges through the exocyclic O atom. The three metal sites attached to the O atom are: the metal vertex to which the N atom is bound (e.g., Ni8), the other vertex forming a side of the trigonal prism (e.g., Ni11) and a metal site capping a square face of the trigonal prism (e.g. Ni5). The six μ_3-O donors from the pyridonate ligands therefore occupy the six triangular faces around the "waist" of the tricapped trigonal prism, that is they centre the faces bounded by one cap and two vertex metal sites.

The chloroacetates bridge in a 1,3-fashion between cap and vertex sites, with each cap attached to two chloroacetate ligands. For example, carboxylates bridge between Ni4 and Ni10, and Ni4 and Ni9. The result of these various bridges is to create a central $[M_{10}(\mu_3\text{-}OH)_6(\eta^2,\mu_3\text{-}xhp)_6(\eta^2,\mu_2\text{-}O_2CR)_6]^{2+}$ fragment, and this fragment recurs in **3** to **9**, differing only in the carboxylates and pyridonates present.

Table 1. Analytical data[a] for compounds **2** to **11**.

Compound	Formula	C	H	N
2	$[Ni_{12}(OH)_6(mhp)_{12}(O_2CCH_2Cl)_6]$	37.7 (37.8)	3.2 (3.4)	6.3 (6.3)
3	$[Ni_{11}(OH)_6(chp)_9(O_2CPh)_6(EtOH)_3][Ni(chp)_3]$	39.4 (40.2)	2.9 (3.0)	4.8 (5.0)
4	$[Ni_{11}(OH)_6(mhp)_9(O_2CMe)_6(H_2O)_3]_2[CO_3]$	37.9 (38.1)	3.6 (3.9)	5.8 (5.8)
5	$[Ni_{11}(OH)_6(mhp)_9(O_2CMe)_7(Hmhp)_2]$	40.6 (40.8)	3.7 (4.0)	6.5 (6.6)
6	$[Ni_{10}(OH)_6(mhp)_{6.5}(O_2CCHMe_2)_{6.5}(Hmhp)_3Cl(H_2O)]$	42.1 (42.6)	5.6 (4.9)	6.0 (5.7)
7	$[Ni_{10}(OH)_6(chp)_6(O_2CCHPh_2)_6(Cl)_2(Hchp)(H_2O)_2(MeOH)]$	47.1 (48.1)	3.3 (3.4)	3.7 (3.3)
8	$[Co_{10}(OH)_6(mhp)_6(O_2CPh)_7(Hmhp)_3Cl(MeCN)]$	49.0 (48.9)	3.9 (4.0)	4.9 (5.2)
9	$[Co_{10}(OH)_6(mhp)_6(O_2CCMe_3)_7Cl(MeCN)_3(Hmhp)]$	42.6 (43.1)	5.1 (5.3)	4.9 (6.0)
10	$[Ni_{10}(OH)_4(mhp)_{10}(O_2CCMe_3)_6(MeOH)_2]$	48.9 (48.9)	5.2 (5.3)	5.4 (5.4)
11	$[Ni_{10}(OH)_4(mhp)_{10}(O_2CCMe_3)_6(H_2O)_2]$	45.7 (45.4)	4.8 (5.1)	5.3 (5.9)
12	$[Co_{10}(OH)_4(chp)_{10}(O_2CCMe_3)_6(EtOH)_2]\cdot 0.3\,MeOH$	40.7 (40.4)	4.6 (4.0)	5.4 (5.6)

[a] Calculated values are given in parentheses.

0947-6539/00/0605-0884 $ 17.50+.50/0 *Chem. Eur. J.* **2000**, *6*, No. 5

Table 2. Experimental data for the X-ray diffraction studies of compounds **2**–**12**.

Compound	**2**	**3**	**4**	**5**	**6**	**7**
formula	$C_{84}H_{90}Cl_6N_{12}Ni_{12}O_{30}\cdot 0.43\,C_4H_8O_2$	$C_{108}H_{89}Cl_{12}N_{12}Ni_{12}O_{33}\cdot C_4H_{10}O\cdot CH_2Cl_2$	$C_{66}H_{84}N_9Ni_{11}O_{30}\cdot 0.5\,CO_3\cdot 2\,H_2O\cdot 0.5\,C_4H_{10}O$	$C_{80}H_{95}N_{11}Ni_{11}O_{31}\cdot 3\,CH_2Cl_2\cdot 2.75\,H_2O$	$C_{83}H_{113.5}ClN_{9.5}Ni_{10}O_{29.5}$	$C_{120}H_{102}Cl_9N_7Ni_{10}O_{28}\cdot 1.6\,CH_4O\cdot 0.4\,H_2O\cdot 0.4\,C_2H_3N$
M	2702.8	3371.9	2228.3	2176.40	2338.88	3071.14
crystal system	monoclinic	rhombohedral	monoclinic	triclinic	monoclinic	monoclinic
space group	$P2_1/c$	$R3c$	$C2/c$	$P\bar{1}$	$P2_1/c$	$C2/c$
a [Å]	28.278(7)	16.279(3)	39.931(13)	15.223(7))	16.665(4)	12.766(3)
b [Å]	15.118(5)		25.516(10)	16.362(7)	21.371(3)	35.098(6)
c [Å]	28.708(8)	85.61(3)	22.43(2)	24.052(12)	30.940(4)	30.383(6)
α [°]				78.39(5)		
β [°]	114.62(2)		120.2(3)	83.27(2)	105.497(12)	99.34(2)
γ [°]				72.30(2)		
U [Å^3]	11157(6)	19647(8)	19751(17)	5580(2)	10619(3)	13433(5)
T [K]	220.0(2)	150.0(2)	150.0(2)	150.0(2)	220.0(2)	220.0(2)
Z	4	6[c]	8	2	4	4[d]
ρ_{calcd} [g cm^{-3}]	1.609	1.710	1.50	1.295	1.463	1.519
crystal shape and colour	green block	green block	irregular green wedge	green lath	green block	green block
crystal size [mm]	$0.39\times 0.35\times 0.31$	$0.46\times 0.39\times 0.35$	$0.50\times 0.20\times 0.14$	$0.51\times 0.23\times 0.16$	$0.27\times 0.08\times 0.04$	$0.49\times 0.39\times 0.20$
μ/mm^{-1}	2.194	5.104	2.12	2.014	2.712	1.620
unique data	12037	3543	12879	14566	9646	7154
unique data with $F_o > 4\sigma(F_o)$	7845	3355	6174	10342	5318	3316
parameters	1305	560	1089	1279	755	525
max. Δ/σ ratio	0.004	0.005	0.018	0.002	0.014	0.036
$R1$, $wR2$[a]	0.0610, 0.1680	0.0491, 0.1399	0.0938, 0.2797	0.0620, 0.1643	0.1014, 0.3211	0.1040, 0.3075
weighting scheme,[b] w^{-1}	$\sigma^2(F_o^2)+(0.0772\,P)^2+8.0826\,P$	$\sigma^2(F_o^2)+(0.0864\,P)^2+128.2114\,P$	$\sigma^2(F_o^2)+(0.1279\,P)^2+212.030\,P$	$\sigma^2(F_o^2)+(0.0767\,P)^2+17.5823\,P$	$\sigma^2(F_o^2)+(0.0153\,P)^2+106.0031\,P$	$\sigma^2(F_o^2)+(0.1509\,P)^2$
goodness of fit	1.051	1.078	1.019	1.071	1.022	1.028
largest residuals [e Å^{-3}]	+0.783, −0.517	+0.755, −0.583	+1.32 −0.84	+1.18, −0.82	+0.971, −0.607	+1.075, −0.666

The metal sites are each six-coordinate, with the central metal bonded exclusively to μ_3-hydroxide ligands. The capping sites, (Ni4, Ni5 and Ni6), are bonded to two μ_3-hydroxide ligands, two μ_3-O atoms from mhp, and two oxygens derived from carboxylates. The vertex sites (Ni7, Ni8, Ni9, Ni10, Ni11 and Ni12) are bound to only five donors from within this central fragment: one μ_3-hydroxide ligand, two μ_3-O atoms from mhp, one oxygen from a carboxylate and one N-donor atom from an mhp ligand. The final coordination site for these vertex metals is where the structural variation in these cages takes place. In **2** six μ_2-O atoms from mhp ligands each occupy one of these sites, with these ligands part of two $[Ni(mhp)_3]^-$

Table 3. Bond length ranges [Å] for metal sites for compounds **2**–**9**.

	2	**3**	**4**	**5**	**6**	**7**	**8**	**9**
metal and nuclearity	Ni_{12}	Ni_{11}	Ni_{11}	Ni_{11}	Ni_{10}	Ni_{10}	Co_{10}	Co_{10}
bonds involving central metal atom								
M–OH	2.048–2.054	2.057–2.075	2.057–2.095	2.044–2.069	2.034–2.091	2.056–2.067	2.080–2.115	2.085-2.129
bonds involving metal atoms at vertices of trigonal prism								
M–OH	1.932–1.948	1.950–1.993	1.935–1.994	1.934–1.976	1.934–1.972	1.944–1.979	1.962–2.025	1.963–2.004
M–N(xhp)	2.041–2.065	2.071–2.137	2.050–2.115	2.063–2.102	2.049–2.083	2.065–2.091	2.090–2.154	2.077–2.140
M–μ_3-O(xhp)	2.177–2.308	2.132–2.255	2.093–2.247	2.131–2.272	2.110–2.277	2.119–2.258	2.158–2.335	2.165–2.516
M–O(bridging O_2CR)	2.002–2.043	1.968–2.012	1.981–2.040	1.983–2.027	1.984–2.049	1.999–2.012	2.013–2.066	2.018–2.045
M–μ_2-O (from $[Ni(xhp)_3]$)	2.116–2.146	2.115	2.094–2.148	2.113–2.155	none	none	none	none
M–O(Hxhp)	none	none	none	2.036–2.060	2.062–2.110	2.049	2.076–2.163	2.090
M–Cl	none	none	none	none	2.404	2.392	2.483–2.533	2.456
M–O(terminal O_2CR)	none	none	none	2.037	2.074	none	2.035	2.077
M–N(solvent)	none	none	none	none	none	none	2.156	2.127–2.270
M–O(solvent)	none	2.044	2.018–2.053	none	2.074	2.226	none	none
bonds involving metal atoms capping square faces of trigonal prism								
M–OH	2.001–2.018	1.993–2.078	1.977–2.087	1.987–2.046	1.997–2.040	2.016–2.060	2.043–2.093	2.042–2.087
M–μ_3-O(xhp)	2.098–2.155	2.154–2.163	2.118–2.199	2.107–2.155	2.096–2.152	2.111–2.178	2.149–2.202	2.169–2.207
M–O(bridging O_2CR)	2.015–2.047	1.994–2.047	2.012–2.038	2.008–2.056	2.016–2.044	2.007–2.037	2.005–2.048	2.021–2.059
bonds involving metal atoms capping trigonal faces of trigonal prism, that is in $[Ni(xhp)_3]$ units								
M–N(xhp)	2.027–2.058	2.043–2.075	2.009–2.039	2.031–2.055	none	none	none	none
M–μ_2-O(xhp)	2.215–2.262	2.106–2.188	2.218–2.225	2.237–2.245	none	none	none	none
average esds.	0.007	0.007	0.013	0.006	0.011	0.012	0.008	0.010

Table 2. cont.

Compound	**8**	**9**	**10**	**11**	**12**
formula	$C_{105}H_{101}ClCo_{10}N_{12}O_{29}\cdot 1.5\,C_2H_3N$	$C_{82}H_{121}ClCo_{10}N_{10}O_{27}\cdot C_2H_3N$	$C_{92}H_{126}N_{10}Ni_{10}O_{28}\cdot 0.58\,CH_4O$	$C_{90}H_{122}N_{10}Ni_{10}O_{28}\cdot 1.85\,C_2H_3N\cdot 0.65\,H_2O$	$C_{84}H_{100}Cl_{10}N_{10}Co_{10}O_{28}\cdot 0.3\,CH_4O$
M_r	2653	2356.7	2425.8	2466.7	2649.9
crystal system	triclinic	monoclinic	rhombohedral	monoclinic	monoclinic
space group	$P\bar{1}$	$P2_1/c$	$R\bar{3}c$	$P2_1/n$	$P2_1/n$
a [Å]	15.995(6)	16.784(2)	52.372(10)	17.005(3)	15.5744(3)
b [Å]	16.176(7)	21.672(3)		27.670(6)	26.1387(4)
c [Å]	25.275(14)	30.972(4)	21.805(6)	26.474(6)	27.3620(5)
α [°]	88.84(3)				
β [°]	85.33(4)	98.38(2)		96.75(2)	93.6096(8)
γ [°]	61.21(3)				
U [Å^3]	5711(4)	11146(2)	51795(20)	12370(5)	11116.8(3)
T [K]	150.0(2)	220.0(2)	220.0(2)	220.0(2)	150.0(2)
Z	2	4	18[d]	4	4
ρ_{calcd} [g cm^{-3}]	1.542	1.404	1.400	1.324	1.583
crystal shape and colour	pink plate	red tablet	green block	green plate	red block
crystal size [mm]	$0.47\times 0.39\times 0.04$	$0.31\times 0.23\times 0.16$	$0.39\times 0.35\times 0.31$	$0.58\times 0.39\times 0.04$	$0.2\times 0.2\times 0.3$
μ [mm^{-1}]	1.515	1.541	2.309	2.162	1.760
unique data	9600	15583	8106	17157	23571
unique data with $F_o > 4\sigma(F_o)$	6038	7414	4818	9895	11132
parameters	1429	1191	627	1329	1255
max. Δ/σ ratio	−0.031	0.066	−0.007	0.039	0.031
$R1$, $wR2$[a]	0.0698, 0.1807	0.0864, 0.2315	0.0684, 0.2094	0.0814, 0.2654	0.0787, 0.1853
weighting scheme[b], w^{-1}	$\sigma^2(F_o^2)+(0.0312\,P)^2+35.211\,P$	$\sigma^2(F_o^2)+(0.0667\,P)^2+32.0753\,P$	$\sigma^2(F_o^2)+(0.1011\,P)^2$	$\sigma^2(F_o^2)+(0.1554\,P)^2$	$\sigma^2(F_o^2)+(0.1660\,P)^2$
goodness of fit	0.930	1.062	1.015	0.994	1.009
largest residuals [e Å^{-3}]	+0.837, −0.550	+0.628, −0.502	+0.737, −0.640	+1.022, −0.838	1.237, −1.539

[a] $R1$ based on observed data, $wR2$ on all unique data. [b] $P = 1/3[\max(F_o^2, 0) + 2F_c]$. [c] The molecule lies on a three-fold axis. [d] The molecule lies on a two-fold axis.

fragments (containing Ni2 and Ni3) which occupy both the upper and lower triangular faces of the trigonal prism. Thus the $[Ni(mhp)_3]^-$ fragments could be regarded as trinucleating "ligands".

$[Ni_{11}(OH)_6(chp)_9(O_2CPh)_6(EtOH)_3][Ni(chp)_3]$ (**3**) is shown in Figure 3, and was formed unexpectedly and in 15% yield. It crystallises with a crystallographic three-fold axis coincident with the trigonal axis of the cage. Many of the features described for **2** can be recognised, including the central $[M_{10}(\mu_3\text{-}OH)_6(\eta^2,\mu_3\text{-}xhp)_6(\eta^2,\mu_2\text{-}O_2CR)_6]^{2+}$ fragment. In **3** the pyridonate ligand present is 6-chloro-2-pyridonate (chp), which is one of only two examples we have of this ligand stabilising a tricapped-trigonal prism. The carboxylate ligand present is benzoate. The functions adopted by the pyridonate and carboxylates within this core are identical to those found in **2**.

The significant change between **2** and **3** is the ligation on one of the triangular faces. In **3** three molecules of

Table 4. Bond angle ranges [°] for metal sites for compounds **2**–**9**.

	2	**3**	**4**	**5**	**6**	**7**	**8**	**9**
metal and nuclearity	Ni_{12}	Ni_{11}	Ni_{11}	Ni_{11}	Ni_{10}	Ni_{10}	Co_{10}	Co_{10}
angle ranges involving central metal atom								
cis angles	79.0–109.8	81.5–93.5	81.3–104.3	76.7–106.5	80.6–106.2	81.2–106.2	80.6–110.1	81.1–105.5
trans angles	157.9–158.4	162.8	162.0–164.0	159.6–161.4	161.8–161.9	161.9–163.7	158.6 162.6	160.6–165.6
angle ranges involving metal atoms at vertices of trigonal prism								
cis angles between O,N-donors of chelating xhp	60.6–61.8	61.5–62.1	60.6–62.8	60.8–62.7	60.8–61.9	60.9–62.0	60.1–61.1	58.0–61.2
other *cis* angles	75.2–104.1	74.8–101.5	75.4–104.1	72.9–105.6	75.3–103.4	75.2–102.5	77.2–105.7	76.2–106.6
trans angles	155.8 -165.4	157.7–176.2	157.2–172.2	155.9–171.2	157.6–167.6	160.1–166.6	155.2–166.4	150.7–172.5
angle ranges involving metal atoms capping square faces of trigonal prism								
cis angles	75.7–97.7	76.4–98.1	74.2–100.1	73.2–99.9	75.3–100.9	75.4–97.6	76.6–97.6	75.9–99.2
trans angles	162.5–173.0	163.2–174.2	163.6–173.9	161.8–174.2	160.5–172.8	165.3–173.8	163.4–173.7	163.2–175.6
angle ranges involving metal atoms capping trigonal faces of trigonal prism								
cis angles between O,N donors of chelating xhp	61.4–62.8	62.5–65.3	62.6–63.0	62.0–62.7				
other *cis* angles	92.5–106.4	95.4–103.5	91.8–105.6	92.8–105.0				
trans angles	157.4–161.9	157.9–159.0	159.4–162.7	158.0–161.0				
average esds.	0.3	0.3	0.5	0.2	0.4	0.5	0.3	0.4

0947-6539/00/0605-0886 $ 17.50+.50/0 *Chem. Eur. J.* **2000**, *6*, No. 5

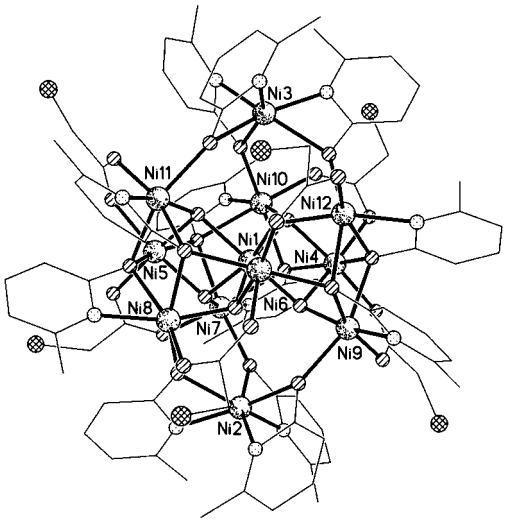

Figure 1. Compound **2** viewed perpendicular to the trigonal axis of the prism. The upper trigonal face of the prism is defined by Ni10, Ni11 and Ni12, the lower by Ni7, Ni8 and Ni9. Ni1 is at the centre of the polyhedron and Ni4, Ni5 and Ni6 cap the rectangular faces. In all figures the following shading is used: Ni or Co, heavy random dots; Cl, cross-hatched; N, light dotted; O, diagonal-shading top-right to bottom left; C shown as lines. H-atoms are not included for clarity.

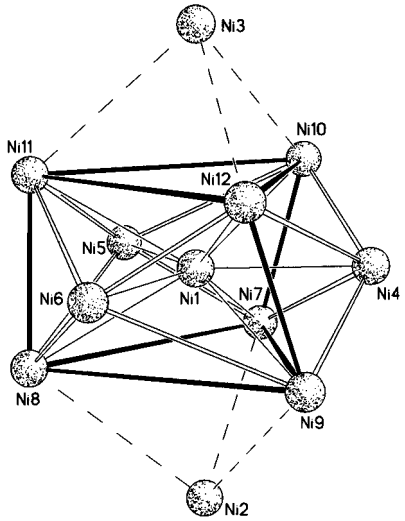

Figure 2. The centred-pentacapped trigonal prismatic core of **2**.

EtOH—carried forward from the first step of the synthesis—are bound to Ni3 and its symmetry equivalents, thus displacing the cap. A $[Ni(chp)_3]^-$ fragment (containing Ni6) is hydrogen-bonded to these EtOH molecules, and has a very similar coordination geometry to the $[Ni(mhp)_3]^-$ fragments in **2**. The O···O distance for these H bonds is 2.603(10) Å. This O···O distance, and others mentioned below, is similar to those found in crystal structures of carboxylic acids.[11] The other triangular face of the prism has retained a $[Ni(chp)_3]^-$ cap (containing Ni4), attached through three μ_2-O atoms from chp to Ni2 and its symmetry equivalents. Compound **3** can therefore be regarded as an intermediate structure between a dodecanuclear pentacapped-centered-trigonal prism and an undecanuclear tetracapped-centered-trigonal prism.

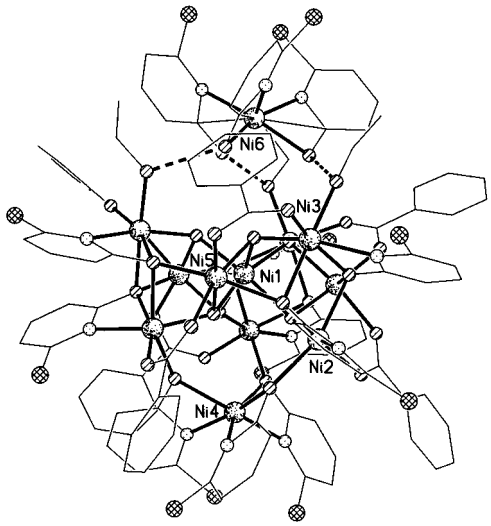

Figure 3. Compound **3** viewed perpendicular to the trigonal axis, showing the hydrogen bonding between the $[Ni(chp)_3]$ fragment containing Ni12 and the Ni_{11} cage. A crystallographic C_3 axis passes through Ni4, Ni1 and Ni6. The upper face of the prism is defined by Ni3 and symmetry equivalents, the lower by Ni2. Ni1 is at the centre of the polyhedron and Ni5 and symmetry equivalents.

The synthesis for both **4** and **5** is different from the procedure used for the other cages reported here. Nickel acetate was used as a starting material rather than nickel

$[Ni_{11}(OH)_6(mhp)_9(O_2CMe)_6(H_2O)_3]_2[CO_3]$ **4**

$[Ni_{11}(OH)_6(mhp)_9(O_2CMe)_7(Hmhp)_2]$ **5**

chloride, and, after initial reaction of nickel acetate with Na(mhp) in either THF or MeOH, further Hmhp was added to the solid produced by evaporation of these solutions prior to crystallisation from CH_2Cl_2.

Both **4** and **5** contain undecanuclear cages, however they differ in the ligation on the uncapped triangular face. In **4** the three sites on this face, one each on Ni2, Ni6 and Ni9, are occupied by three water molecules. This creates a very hydrophilic face for the cage and in the crystal two molecules of **4** interact through six hydrogen bonds to produce a dimer of undecanuclear cages (Figure 4). The six hydrogen bonds have O···O distances of between 2.565 and 2.896(12) Å. Compound **4** is also the only compound in this series which crystallises as a cation. The counter-ion is a carbonate ion, which we believe has formed from atmospheric CO_2 during crystallisation. In **5** (Figure 5), the three coordination sites on this face are occupied by one acetate and two Hmhp ligands which supply the three O donors required to make the three Ni atoms (Ni5, Ni7 and Ni11) in this face six-coordinate. There are no significant intermolecular interactions in **5**.

$[Ni_{10}(OH)_6(mhp)_{6.5}(O_2CCHMe_2)_{6.5}(Hmhp)_3Cl(H_2O)]$ (**6**) contains a decanuclear cage, and has a structure similar to **7**, which is shown in Figure 6. The reaction is identical to that used to produce **2** except that the carboxylate ligand present is isobutyrate rather than chloroacetate. The decanuclear cage lacks both caps on the triangular faces, but the connectivity within the $[M_{10}(\mu_3\text{-}OH)_6(\eta^2, \mu_3\text{-}xhp)_6(\eta^2, \mu_2\text{-}O_2CR)_6]^{2+}$ core is essentially unaltered from the similar fragment found in **2**–**5**.

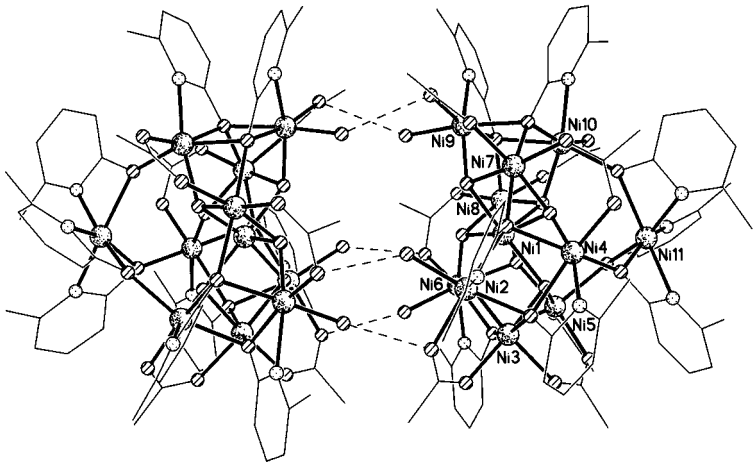

Figure 4. A dimer of Ni_{11} cages in **4** viewed perpendicular to the trigonal axis, showing the hydrogen bonding between neighbouring Ni_{11} cages. The trigonal faces of the prism are defined by Ni6, Ni2 and Ni9 and Ni5, Ni4 and Ni10, with Ni1 at the centre of the polyhedron and Ni3, Ni7 and Ni8 capping the rectangular faces.

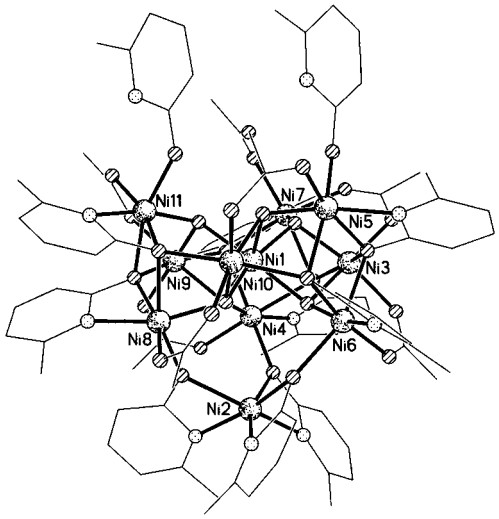

Figure 5. Compound **5** viewed perpendicular to the trigonal axis of the prism. The upper face of the prism is defined by Ni5, Ni7 and Ni11, the lower by Ni4, Ni6 and Ni8, with Ni1 at the centre of the polyhedron and Ni3, Ni9 and Ni10 capping the rectangular faces.

The absence of both caps creates three coordination sites on the upper and lower triangular faces of the prism. One of these faces is occupied by one chloride and two O-bound Hmhp ligands. The coordination sites on the second face are occupied by a disordered mixture of one water, one Hmhp, a half-occupancy isobutyrate ligand and a half-occupancy mhp ligand. The methyl groups of the isobutyrate ligands all show considerable thermal motion consistent with some disorder. It is unclear why the groups coordinated to this face are disordered, however it is not due to twinning or any other crystallographic problem. Similar disorder is found in **8** (see below). A similar decanuclear cage (**7**) (Figure 6), results if diphenylacetate is used. As in **3** the 6-chloro-2-pyridonate ligand is present rather than mhp, but this does not effect the bridging within the core. The upper and lower faces are coordinated by two chloro ligands, an Hchp, two water molecules and a MeOH solvate.

$[Ni_{10}(OH)_6(chp)_6(O_2CCHPh_2)_6(Cl)_2(Hchp)(H_2O)_2(MeOH)]$ **7**

$[Co_{10}(OH)_6(mhp)_6(O_2CPh)_7(Hmhp)_3Cl(MeCN)]$ **8**

Although we have been unable to synthesise crystalline samples of dodeca- or undecanuclear cages containing cobalt(II), we have made two decanuclear tricapped trigonal prismatic cobalt cages. Compound **8** is formed by using sodium benzoate as a reactant (Figure 7). As in **6** the $[M_{10}(\mu_3\text{-}OH)_6(\eta^2,\mu_3\text{-}xhp)_6(\eta^2,\mu_2\text{-}O_2CR)_6]^{2+}$ core is regular and ordered, but the ligands attached to one of triangular faces of the prism are disordered. In **7** one triangular face is occupied by one benzoate ligand, one Hmhp and one MeCN with no disorder, while the other face is occupied by two Hmhp

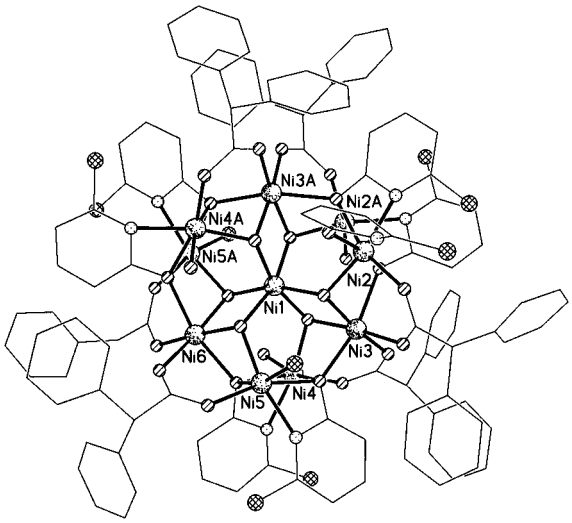

Figure 6. Compound **7** viewed down the trigonal axis of the prism.

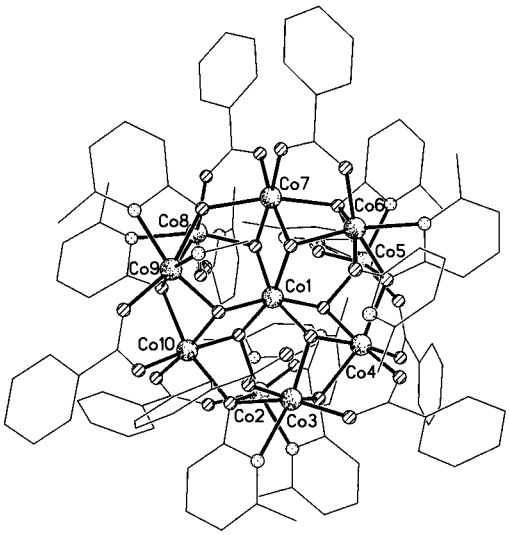

Figure 7. Compound **8** viewed down the trigonal axis of the prism.

0947-6539/00/0605-0888 $ 17.50+.50/0 *Chem. Eur. J.* **2000**, *6*, No. 5

ligands and one chloro ligand, disordered over the three Co atoms within the face. In **9** the arrangement of ligands on these

$[Co_{10}(OH)_6(mhp)_6(O_2CCMe_3)_7Cl(MeCN)_3(H_2O)]$ **9**

faces is ordered, with the "upper face" occupied by two MeCN and one trimethylacetate ligands, and the "lower" face occupied by one chloride, one MeCN and one water ligand. It is worth noting that one of the cobalt sites at the vertex of the trigonal prism (Co9) verges on five-coordinate, with the Co–O bond to the O donor in the sixth coordination site 2.516(10) Å. This is some 0.3 Å longer than equivalent bonds in other structures.

While **9** is clearly related to the other trigonal prisms, use of trimethylacetate can lead to markedly different structures. For nickel two cages, **10** and **11**, have been crystallised

$[Ni_{10}(OH)_4(mhp)_{10}(O_2CCMe_3)_6(MeOH)_2]$ **10**

$[Ni_{10}(OH)_4(mhp)_{10}(O_2CCMe_3)_6(H_2O)_2]$ **11**

from reactions involving nickel chloride, Na(mhp) and $Na(O_2CCMe_3)$. The structure of **10** is shown in Figure 8, and **11** differs chemically only in the presence of two terminal water ligands, rather than two terminal methanol ligands. Bond lengths and angles for these two cages are given in Tables 5 and 6 respectively. In the following the numbering for **10** is given in the text, with the numbering for the equivalent metal sites in **11** given in brackets.

Compound **10** crystallises with a two-fold axis passing through Ni1 and Ni2 and is held together by four μ_3-OH ligands, six 1,3-bridging carboxylates and ten pyridonate ligands. In **11** the crystallographic two-fold axis is absent, however Ni1 and Ni2 still lie on the central axis of the cage. The metal array does not describe a complete polyhedron, however "virtual" addition of further vertices reveals a centred 14-vertex deltahedron as shown in Figure 9. The five missing vertices delineate an equatorial fissure, as if the deltahedron had been cut through the centre with the two

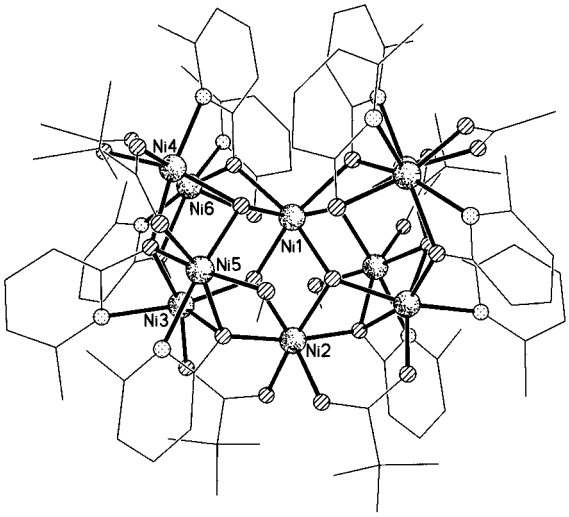

Figure 8. Compound **10** viewed perpendicular to the crystallographic two-fold axis passing through Ni1 and Ni2.

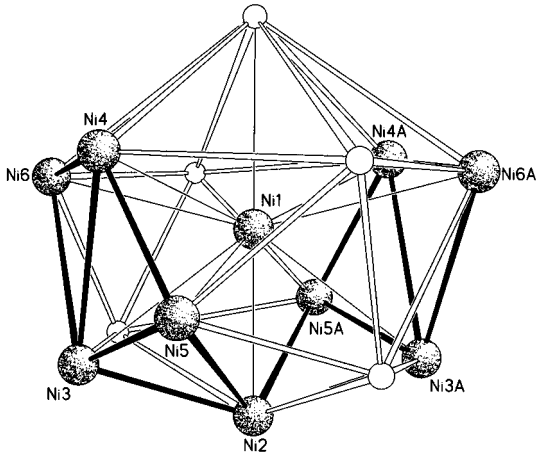

Figure 9. The core of **10** displayed as an incomplete tetraicosahedron. The additional vertices required to complete the polyhedron are shown as open circles.

Table 5. Bond length ranges [Å] for metal sites in compounds **10**–**12**.

	10	**11**	**12**
bonds involving central metal atom	M = Ni1	M = Ni1	M = Co1
M–OH	2.025–2.049	2.034–2.047	2.019–2.072
M–O(mhp)	2.269	2.237–2.238	2.389–2.404
bonds involving cap on lower hexagon	M = Ni2	M = Ni2	M = Co2
M–OH	2.061	2.068–2.075	2.085–2.101
M–O(mhp)	2.061	2.074	2.174–2.181
$M–O(O_2CCMe_3)$	2.009	2.029–2.0323	2.024–2.047
bonds involving metals in lower hexagon	M = Ni3, Ni5	M = Ni3, Ni4, Ni8, Ni9	M = Co3, Co4, Co8, Co9
M–OH	2.000–2.033	1.989–2.075	2.015–2.090
M–O(mhp)	2.006–2.185	1.997–2.183	2.051–2.254
M–N(mhp)	2.093–2.143	2.100–2.118	2.142–2.198
$M–O(O_2CCMe_3)$	1.996–1.999	1.981–2.004	2.004–2.016
M–O(solvent)	2.059	2.053–2.063	2.059–2.072
bonds involving metals in upper hexagon	M = Ni4, Ni6	M = Ni5, Ni6, Ni7, Ni10	M = Co5, Co6, Co7, Co10
M-OH	2.058	2.053–2.057	2.084–2.099
M–O(mhp) "short"	2.025–2.137	2.048–2.158	2.109–2.178
M–O(mhp) "long"	2.423	2.421–2.436	2.344–2.373
M–N(mhp)	2.037–2.093	2.029–2.117	2.107–2.176
$M–O(O_2CCMe_3)$	1.996–2.005	1.998–2.014	1.987–2.205
average esds.	0.005	0.007	0.005

Table 6. Bond angle ranges [°] for metal sites in compounds **10**–**12**.

	10	**11**	**12**
angle ranges involving central metal atom	Ni1	Ni1	Co1
cis angles	82.2–105.1	82.2–103.5	88.0–103.7
trans angles	165.0–167.0	167.1–167.9	159.4–166.3
angle ranges involving cap on lower hexagon	Ni2	Ni2	Co2
cis angles	77.0–97.0	77.0–96.3	77.5–98.0
trans angles	168.3–169.6	167.8–170.4	166.3–168.4
angle ranges involving metals in lower hexagon	Ni3, Ni5	Ni3, Ni4, Ni8, Ni9	Co3, Co4, Co8, Co9
cis angles between O,N donors of chelating xhp	61.8–63.2	62.1–62.5	60.5–61.5
other *cis* angles	76.4–101.2	77.0–102.3	78.1–103.5
trans angles	159.2–168.2	159.5–169.7	156.7–164.8
angle ranges involving metals in upper hexagon	Ni4, Ni6	Ni5, Ni6, Ni7, Ni10	Co5, Co6, Co7, Co10
cis angles between O,N donors of chelating xhp	60.0–63.5	59.7–63.4	59.8–61.5
other *cis* angles	77.4–103.4	77.0–104.9	77.1–107.7
trans angles	153.8–165.6	153.8–169.4	143.8–165.2
average esds.	0.2	0.3	0.2

sides falling apart slightly. Given the absence of so many vertices the overall geometry is surprisingly regular with Ni1 (Ni1) at the centre, Ni3, Ni3A, Ni5 and Ni5A (Ni3, Ni4, Ni8, Ni9) occupying four of the vertices of one hexagon and Ni4, Ni4A, Ni6 and Ni6A (Ni5, Ni6, Ni7, Ni10) four of the vertices of the second hexagon. Ni2 (Ni2) caps the former hexagon.

The mhp ligands present adopt four different coordination modes: chelating to Ni6 (Ni6, Ni10); chelating to Ni6 (Ni6, Ni10) while bridging through the O atom to Ni3 (Ni3, Ni8); chelating to Ni3 (Ni3, Ni8) or Ni5 (Ni4, Ni9) and bridging through the O atom to two further atoms Ni4 (Ni5, Ni7) and Ni5 (Ni4, Ni9) or Ni2 (Ni2) and Ni3 (Ni3, Ni8), respectively; binding to Ni4 (Ni5, Ni7) through the ring nitrogen and bridging two further Ni sites, Ni1 (Ni1) and Ni6 (Ni6, Ni10), through the oxygen donor. The mhp ligand therefore shows a much more diverse coordination chemistry in **10** and **11** than in the structures based on tricapped-trigonal-prisms. The three crystallographically independent carboxylates all act as 1,3-bridges between Ni4 (Ni5, Ni7) and Ni6 (Ni6, Ni10), Ni2 (Ni2) and Ni3 (Ni3, Ni8), and Ni4 (Ni5, Ni7) and Ni5 (Ni4, Ni9).

The metal coordination sites are more diverse than in the tricapped-trigonal prism (ttp) structures, with the six independent sites chemically non-equivalent. Ni1 (Ni1) is bound to four μ_3-hydroxide ligands, and two μ_2-oxygen atoms from mhp ligands. Ni2 (Ni2) lies at the base of the tetraicosahedron and is bound to two μ_3-hydroxide ligands, two μ_3-O atoms from mhp, and two carboxylate oxygen atoms. Ni3 (Ni3, Ni8) is bound two chelating mhp ligands, one μ_3-hydroxide ligand and one carboxylate oxygen atom; Ni4 (Ni5, Ni7) is only five-coordinate, bound to one N-donor from an mhp ligand, one μ_3-hydroxide ligand, one μ_3-oxygen atom from an mhp, and two oxygen atoms from carboxylates; Ni5 (Ni4, Ni9) is bound to two μ_3-hydroxide ligands, one chelating mhp ligand, one carboxylate oxygen atom and the terminal MeOH group; Ni6 (Ni6, Ni10) is bound to two chelating mhp ligands, one further mhp oxygen atom and one carboxylate oxygen atom.

A further example of this tetraicosahedral core is found in **12**, which also contains the trimethylacetate ligand but is formed with cobalt and chp (Figure 10). Bond lengths and angles for **12** are given in Tables 5 and 6, respectively. The core is identical to that in **10** and **11**, and again there is diversity among both the bonding modes of the ligands and in the metal coordination sites. The chp ligand adopts three coordination modes: the N and O donors chelating a cobalt centre with no further bridging to a metal by the exocyclic oxygen—a mode not found in compounds **2**–**11**; the N and O donors chelating to a Co centre with the O atom binding to a second cobalt; the N and O donors chelating to one Co, with the O atom binding to two further Co atoms. The two chelating pyridonate ligands both form H bonds to coordinated EtOH molecules (O···O 2.506 and 2.525(10) Å). All the carboxylates are present in a 1,3-bridging mode.

Each cobalt atom is six-coordinate with a distorted octahedral geometry. As in **10** and **11** there are six chemically independent sites. Co1 is bound to four μ_3-hydroxide ligands

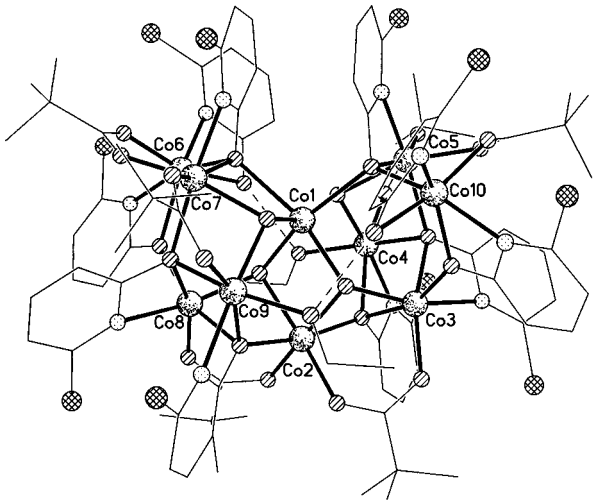

Figure 10. Compound **12** viewed perpendicular to the crystallographic two-fold axis passing through Co1 and Co2.

and two μ_3-oxygen atoms from chp ligands. Co2 is bound to two μ_3-hydroxide ligands, two μ_3-oxygen atoms from chp and two carboxylate oxygen atoms. Co3 and Co8 are each bound to a chelating chp ligand, one μ_3-hydroxide group, a μ_2- and a

$[Co_{10}(OH)_4(chp)_{10}(O_2CCMe_3)_6(EtOH)_2]$ **12**

0947-6539/00/0605-0890 $ 17.50+.50/0 *Chem. Eur. J.* **2000**, *6*, No. 5

μ_3-oxygen atom from chps, and to a carboxylate oxygen atom. Co4 and Co9 are each bound to a chelating chp ligand, one μ_3-hydroxide group, one μ_3-oxygen atom from a chp ligand, one carboxylate oxygen atom and a terminal EtOH molecule. Co5 and Co7 are each bound to one chelating chp group, one μ_3-hydroxide ligand, one μ_3-oxygen atom from a chp ligand, and two carboxylate oxygen atoms. Co6 and Co10 are each bound to two chelating chp ligands, one μ_2-oxygen atom from a chp ligand, and one carboxylate oxygen atom.

Given three examples and moderate yields of this apparently new polyhedron it is difficult to dismiss **10**, **11** and **12** as irrelevant exceptions. Our first thoughts on observing these structures was that the large trimethylacetate ligand was imposing sufficient steric strain on the structure for a reorganisation to be favourable. However the existence of both **9** and **12** raises questions about this assumption. Compound **9** is also a decanuclear cobalt cage which features trimethylacetate, but this has a tricapped-trigonal prismatic core. We have also made two heptanuclear cobalt cages which contain trimethylacetate and chp. [12] There is clearly a fine balance between which structures are formed with which "blend" of ligands. We will return to this question in the discussion.

Magnetic studies: The behaviour of the magnetic susceptibility of compounds **2**, **4** and **7** was studied over the 1.8–250 K temperature range. These results are displayed as plots of $\chi_m T$ against T in Figure 11 (where χ_m is the molar magnetic susceptibility). In each case the magnetic behavior down to around 10 K is typically "ferrimagnetic", that is antiferromagnetic exchange stabilising non-diamagnetic ground states. The multiplicity of these ground states clearly varies dramatically between the three cages. For **2** $\chi_m T$ goes through a maximum at 12 K, where the value is around 45 emu K mol^{-1}. Such a value, allowing for two additional $S=1$ centres in the molecule, is consistent with an $S=8$ ground state for the central centred-tricapped-trigonal prism. For **4** the maximum in $\chi_m T$ is much less dramatic, and the value of 11 emu K mol^{-1} suggests an $S=4$ ground state for the M_{10} core. For **7**, the maximum is almost unnoticeable, and this leads us to believe we have an $S=2$ ground state.

Neither **2** nor **4** has any crystallographic symmetry, and **7** has only a crystallographic two-fold axis passing through it, therefore in principle for each cage there are a very large number of independent exchange interactions. This would lead to the fit being vastly over-parameterised in any computational model. Therefore, we decided to attempt to fit the data for each cage using a common coupling scheme which assumes at least D_3 symmetry for the cage, and which assumes that all the important exchange interactions occur between the ten Ni centres within the tricapped-centred-trigonal prisms and that the predominant super-exchange path is through the μ_3-hydroxide ligands. In **2** two additional Ni centres on the trigonal faces of the prism, and in **4** one additional nickel were considered to be magnetically isolated. These non-interacting magnetic ions were included in the treatment as an additive term to magnetic susceptibility assuming a Curie behaviour with a g factor of 2.2.

The coupling scheme used is illustrated in Figure 12 and corresponds to the Hamiltonian given in Equation (1): one

$$H = J_1 S_1(S_7+S_8+S_9+S_{10}+S_{11}+S_{12}) + J_2 S_1(S_4+S_5+S_6) + J_3[S_4(S_9+S_{10}) + S_5(S_7+S_{11}) + S_6(S_8+S_{12})] \quad (1)$$

coupling constant (J_1) accounts for the interaction between the central Ni^{II} ion and the six Ni ions at the corners of the prism; a second constant (J_2) was added for the coupling of the central ion with the three atoms the capping position; finally, the presence of a coupling (J_3) between the nine nickel atoms in the outer sphere was included. S_i refers to the spin on Ni_i, and the numbering of the Ni centres corresponds to that used for **2**, and illustrated in Figure 12. In all calculations the g factor was maintained constant for all the Ni^{II} ions at 2.2.

Fitting the observed data to the coupling scheme in Figure 12 generates exchange constants for the three cages. The sign convention used is that ferromagnetic exchange constants are negative. For **2** the values obtained are: $J_1 = 11.8$, $J_2 = -3.8$, $J_3 = -6.6$ cm^{-1}. These give a calculated

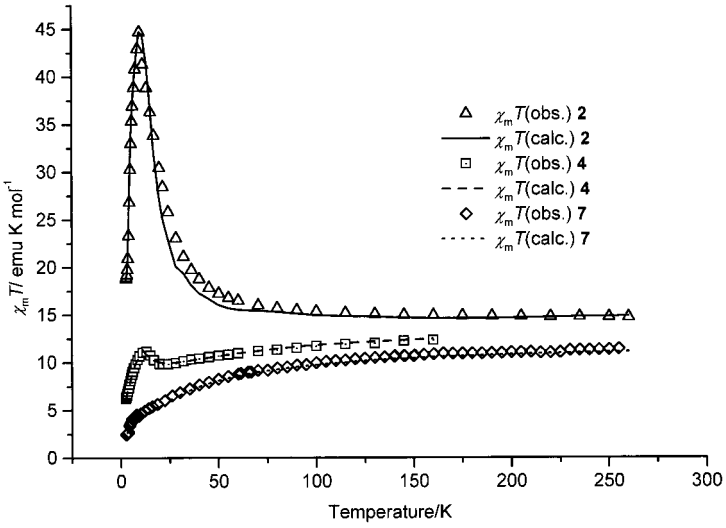

Figure 11. Plot of $\chi_m T$ vs. T for **2**, **4** and **7**.

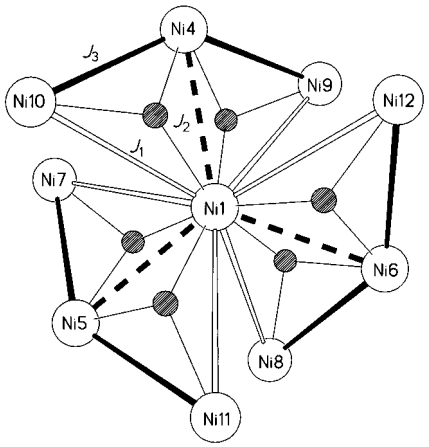

Figure 12. Schematic presentation of the coupling scheme used to model susceptibility data for **2**, **4** and **7**. The cage is viewed down the trigonal axis, and the numbering of the metal centres corresponds with that used for **2**.

ground state of $S=8$ with highly degenerate $S=7$ states some 15 cm^{-1} higher in energy. The fall in $\chi_m T$ below 12 K cannot be modelled using inter-molecular interactions, nor by assuming zero-field splitting of the $S=8$ ground state alone. Instead the model requires inclusion of zero-field splitting parameters for both the $S=8$ state, and the $S=7$ excited states. These parameters come out as $D_{GS}=0.77\ cm^{-1}$ and $D_{ES1}=-0.61\ cm^{-1}$. The calculated values for $\chi_m T$ are shown in Figure 11.

For **4** two different fitting procedures were tried. In the first series of calculations we considered the whole set of data, while in the second series we included only the data from 250 K down to the maximum $\chi_m T$ value. These approaches are based on two different assumptions. The first hypothesis considers the overall magnetic behaviour at all temperatures as due only to intra-molecular interactions, while the second procedure assumes that at low temperature some other mechanism prevails in addition to the intra-cluster one. The first procedure yielded a diamagnetic ground state due to antiferromagnetic interactions with $J_1=9.72(3)\ cm^{-1}$, $J_2=8.81(4)\ cm^{-1}$, $J_3=3.68(4)\ cm^{-1}$. The agreement with experimental data for this model is fair. The second fitting procedure yielded a different set of coupling constants with an alternate ferro-antiferromagnetic nature: $J_1=-19.54(2)\ cm^{-1}$, $J_2=53.18(6)\ cm^{-1}$, $J_3=-1.76(4)\ cm^{-1}$. The calculated ground state has a spin multiplicity $S=4$ and the agreement with the experiment is better, as shown in Figure 11. For this model the low-temperature behaviour could be attributed to three possible causes: i) saturation effects; ii) inter-cluster interactions; iii) zero-field splitting (ZFS) effects. Saturation effects were ruled out by repeating the measurements at smaller external magnetic fields (down to 0.1 T) and no substantial differences in the data sets were observed.

The second possible cause for the fall in $\chi_m T$—inter-cluster coupling—seemed consistent with the crystal structure which shows strong inter-molecular H-bonding giving a dimer of undecanuclear cages. Therefore the magnetic susceptibility below 20 K was calculated to be due to dimers of $S=4$ units using a simple Bleaney–Bowers expression but no reasonable fitting was obtained. Even considering dipolar interactions in a mean field approach failed to give good results.

The ZFS effects were considered by using the energy levels with their spin multiplicity obtained from the second set of calculations. The data were modelled by including ZFS in two ways: firstly only for the ground $S=4$ state which gave a D_{GS} value of 6.97(2) cm^{-1} and an excellent fit to the experimental data, as shown in Figure 11. This substantial value for D_{GS} led us to consider a second model in which the splitting of the first excited state ($S=5$) was included, however the introduction of the second ZFS parameter did not improve the agreement with the experimental data.

For **7** the exchange coupling constants for the best fit to the experimental data are $J_1=6.5$, $J_2=2.5$, $J_3=6.0\ cm^{-1}$, however the first two values can vary within 1 cm^{-1} around these values with little change in the quality of the fit. The calculated ground state has $S=2$, and the calculated curves form a plateau below 6 K: by introducing a ZFS of 4.8 cm^{-1} the final decrease below 6 K of $\chi_m T$ can be reproduced. The calculated values are shown in Figure 11.

Discussion

Structural results

Given the number of related structures it is worthwhile to look for structural trends within the cages. In particular, the change from tricapped-trigonal prism (ttp) structures to the polyhedra observed in **10**, **11** and **12** seemed curious. There are two questions which we have attempted to answer. Firstly **10**, **11** and **12** are structurally related to the ttp structures. Secondly, if **10**, **11** and **12** are related to the ttp cages, can a gradual change be observed in the ttp cores of **1**–**9** as the steric requirements of the carboxylate ligands are increased from acetate to trimethylacetate. This may be manifested in one of two effects, either a distortion of the metal polyhedra, or greater distortion in the coordination geometries of the metal sites.

To answer the first question: careful comparison of the cores of either **1** or **2** with those of **10**, **11** or **12** reveal a greater resemblance than appears from initial observation. Figure 13 illustrates the results of this comparison using the cores of **2** and **11**; for reasons of clarity the metal core of **2** is labelled M1, M2 and so on. Compounds **1** and **2** contain a M_{12} core and eight of the vertices in this core have very close equivalents in **11**. The vertices which match are the central metal M1 which matches with the central nickel Ni1 of **11**; two of the three edges of the prism (M7, M8, M10, M11 which match with Ni3, Ni9, Ni4 and Ni8, respectively); and the three caps on the rectangular faces of the prism (M4, M5, M6 which match with Ni5, Ni2 and Ni7, respectively). The remaining two vertices in **11** (Ni6 and Ni10) appear in the same region as the caps on the trigonal faces of the prism in **1** or **2** (M2 and M3), but are displaced further from them. The only vertices in **1** or **2** which do not have equivalents in **10**, **11** or **12** are the two vertices of one edge of the prism (M9 and M12 in Figure 13).

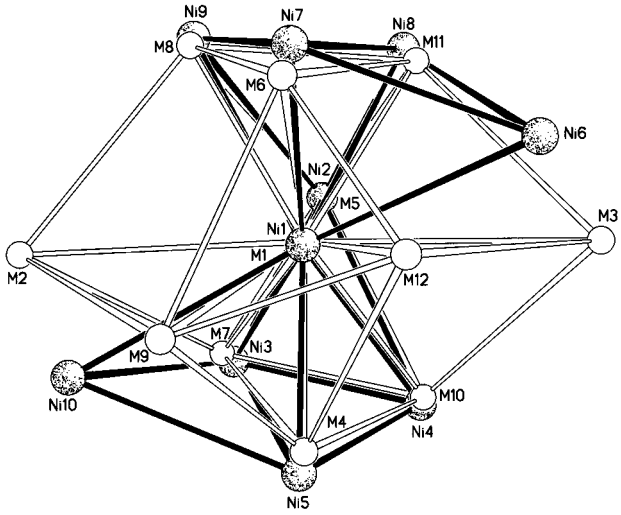

Figure 13. A comparison of the metal cores of **2** and **11**. The sites in **2** are shown as open circles, labelled M1–M12, and are joined through open lines; the sites in **11** are shown shaded with heavy random dots, labelled Ni1–Ni10, and are joined through filled lines. The matching of sites used the OFIT sub-routine in SHELXTL-PC,[13] matching the following pairs of vertices: (M1, Ni1; M4, Ni5; M5, Ni2; M6, Ni7; M7, Ni3; M8, Ni9; M10, Ni4; M11, Ni8).

0947-6539/00/0605-0892 $ 17.50+.50/0 *Chem. Eur. J.* **2000**, *6*, No. 5

Therefore the cores of **10**–**12** could be described as pentacapped-trigonal prisms missing two edge vertices, whereas **7**–**9** are pentacapped-trigonal prisms missing two trigonal caps. Allowing for distortions—and **10**, **11** or **12** are more distorted—all these cages can be derived from the parent polyhedron illustrated in Figure 2. The difference is merely which vertices of the M_{12} are missing. This family resemblance perhaps argues that which cage is found is decided upon by crystallisation conditions, rather than by intramolecular interactions.

The second question—whether the various ttp cores in **1**–**9** are more or less distorted—is more difficult to answer as it is rather difficult to quantify the degree of distortion within a tricapped-trigonal prism without introducing some arbitrary assumptions. We decided as an initial experiment to use the OFIT sub-routine within the SHELXTL-PC package[13] to examine the quality of fit between the central decanuclear polyhedra found in the nine tricapped-trigonal prisms. The results are given in Table 7. The numbers reported are the weighted root mean square (RMS) deviation of the metal sites between structures, and the closest possible match will give a value of zero (as shown for the diagonal terms).

Table 7. Comparison of metal polyhedra found in structures **1**–**9**.

	Dodeca-nuclear cages	Undecanuclear cages			Decanuclear cages			
	1[a]	**2**	**3**	**4**	**5**	**6**	**7**	**8**	**9**
1	0	0.070	0.247	0.201	0.132	0.123	0.102	0.125	0.179
2	0.070	0	0.250	0.204	0.122	0.128	0.106	0.150	0.213
3	0.247	0.250	0	0.060	0.139	0.260	0.215	0.268	0.278
4	0.201	0.204	0.060	0	0.094	0.210	0.166	0.221	0.236
5	0.132	0.122	0.139	0.094	0	0.150	0.104	0.168	0.206
6	0.123	0.128	0.260	0.210	0.150	0	0.074	0.115	0.146
7	0.102	0.106	0.215	0.166	0.104	0.074	0	0.099	0.156
8	0.125	0.150	0.268	0.221	0.168	0.115	0.099	0	0.103
9	0.179	0.213	0.278	0.236	0.206	0.146	0.156	0.103	0

[a] Data taken from reference [5]. All other data this work.

The results demonstrate that there are some differences between the M_{10} cores within the nine structures but it is difficult to see any clear trend. The structures which fit least well with the others are **3**, **4** and **9**. Compounds **3** and **4** are the two undecanuclear cages where there is a strong H-bonded fragment attached to the vacant trigonal face. They match well with each other, less well with **5**, which is also undecanuclear but which lacks any hydrogen bonding to the vacant face, and poorly with the dodeca- and decanuclear cages. Compound **9** contains the pivalate ligand, and it matches well with **8** (the other Co_{10} cage), but less well with **6** or **7** and poorly with all remaining structures. Therefore broadly there are six structures with similar M_{10} cores—**1**, **2**, **5**, **6**, **7** and **8**—and three more distorted cages. It cannot be said that the polyhedron observed in **9** is distorting towards the core observed in **10**, **11** and **12**.

The alternative is that steric strain is causing changes in the coordination spheres of the metal. Examination of bond lengths and angles (Tables 3 and 4) for the structures from **2**–**9** immediately reveals that within each structure the metal–ligand bond lengths at each site vary considerably depending on the ligand, but that equivalent sites in each structure show similar trends. The estimated standard deviations associated with each structure are also given in Tables 3 and 4.

For the metal atoms at the vertices of the trigonal prism the shortest bond is always that to the hydroxide ligand (e.g. for **2**, 1.932–1.948 Å), with the next shortest to the carboxylate oxygen atom (for **2**, 2.002–2.043 Å). The longest bond is that to the O donor of the pyridonate ligand which is chelating to that site (for **2**, 2.270–2.308 Å). One of the two crystallographically independent sites in **3** is the exception to this rule, where the longest bond is to the second pyridonate oxygen bound to this site (2.255 Å) rather than to the O atom of the chelating pyridonate ligand (2.209 Å). This second M–O(xhp) bond is, for all other vertex sites bar one, the second longest bond (for **2** 2.177–2.213 Å). The M–N bond is generally the third shortest (for **2** 2.041–2.065 Å); however, in the undeca- and decanuclear structures this distance is frequently longer than the bond to the terminal ligand derived from solvent or carboxylate. The variation in the coordination of this sixth site on the vertex metals complicates these bond length trends a little.

There is no variation in the ligands coordinated to the metals capping the rectangular faces of the prism. In each case the two longest bonds are those to the pyridonate oxygen atoms (e.g. for **2** 2.098–2.155 Å) with the remaining four bonds—two to hydroxide groups and two to carboxylate groups—having similar values. In some cases, for example **2**, the bonds to OH seem slightly shorter while in other cases, for example **9**, the bonds to carboxylate are shorter, however the difference is barely statistically significant in any case. For the central metal atom in all cases the six bond lengths are statistically identical within the same compound. The metal sites capping the trigonal faces of the prism in all cases have shorter Ni–N bonds than Ni–O bonds.

Summarising the above, it is clear that bonds to pyridonate ligands are, in general longer than bonds involving carboxylate or hydroxide. The most likely explanation of this observation is that the pyridonate ligands are frequently chelating, with a very narrow "bite" angle (ca. 60°) leading to longer bonds from atoms within these chelating groups. There is no statistically significant difference between μ_2- and μ_3-O atoms of pyridonates (see Table 3). It is also noticeable that there is no clear-cut difference between bond lengths involving hydroxide and carboxylate. The longer bonds to pyridonates may explain why the $[Ni(xhp)_3]^-$ "caps" on the trigonal faces of the prism may be displaced while the core structure, which is supported by hydroxide and carboxylate bridges, is maintained.

The presence of different ligands makes comparison between structures difficult; however it is very clear, and probably predictable, that equivalent metal–ligand bonds in the two cobalt structures are longer than those in the six nickel structures. For example, for the central metal sites the Co–O(OH) bonds are, on average, 0.036 Å longer than the Ni–O(OH) bonds, and similar differences are found for all bonds. It is equally clear-cut that for a given metal bond lengths are largely independent of the carboxylate or pyridonate ligand present. These observations may explain why cobalt is able to form a tricapped-trigonal prism with trimethylacetate, but nickel is not; as Co-ligand bonds are

longer any inter-ligand steric repulsion will be weaker as the ligands are necessarily further apart. It is noticeable that in **9** one of the Co–O(mhp) bonds is much longer (2.516(10) Å) than equivalent bonds in the other structures. This bond is to the only cobalt site which has a terminal trimethylacetate ligand attached, so it is tempting to conclude that this elongation is caused by the steric bulk of the trimethylacetate ligand.

The formation of both **9** and **12** with trimethylacetate indicates that these structures must be of very similar stability. The cages were crystallised from different solvents (MeCN for **9** and EtOH for **12**), which suggests the crystallisation step is of importance in controlling which product is formed. It is natural to look for intramolecular controls on structure, for example steric requirements of carboxylate ligands, but here we cannot rule out the formation of different products being largely due to the differing solubility products of the various possible cages in different solvents.

We have commented elsewhere[4] on the extreme coordinative flexibility of the pyridonate ligands, which show eight bonding modes in various polynuclear complexes Within the ttps the variation is much less dramatic (Scheme 1). The ligands which bridge within the $[M_{10}(\mu_3\text{-}OH)_6(\eta^2,\mu_3\text{-}xhp)_6(\eta^2,\mu_2\text{-}O_2CR)_6]^{2+}$ core show only bonding mode **A**, while the ligands involved in the $[Ni(xhp)_3]^-$ caps show bonding mode **B**. Cages **10**–**12** with a core related to a tetraicosahedron, show more variation for the pyridonate bonding modes, with modes **C** and **D** also seen, in addition to **A** and **B**.

Magnetic results: The susceptibility measurements for the three cages studied, **2**, **4** and **7**, reveal that these similar cages have very different spin ground states. In particular the large maximum observed for **2** is best explained by a spin ground state of around $S=8$. The ground states found for **4** and **7** appear to be $S=4$ and $S=2$, respectively. This variation in the susceptibility behaviour is an experimental result, and ideally the computer modelling of the magnetic behaviour would allow us to match this behaviour with structural features.

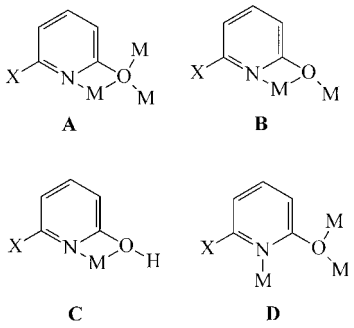

Scheme 1. The bonding modes displayed by pyridonate ligands in complexes **2**–**12**.

However analysis of the structures reveals few statistically significant differences between the three structures (see Table 3 and 4)—other than the obvious change in nuclearity. There is some evidence[14, 15] that the magnitude of exchange coupling in nickel dimers and tetramers can be related to bond angles at bridging groups, however here analysis of the structural data reveals that variation within structures is as great or even greater than that between structures. Change in nuclearity alone could not account for a change of spin ground state from $S=2$ to $S=8$.

The J values calculated by the model allow us to explain the ground states using a very simple picture as shown in Figure 14. The reason for such complex magnetic variations among structurally related cages is because the central Ni centre is involved in M_3 triangles with all the other metals in the ttp cores, with each of J_1, J_2 and J_3 representing the exchange interaction along the edges of the triangle. The balance of these exchange parameters decides the ground state found.

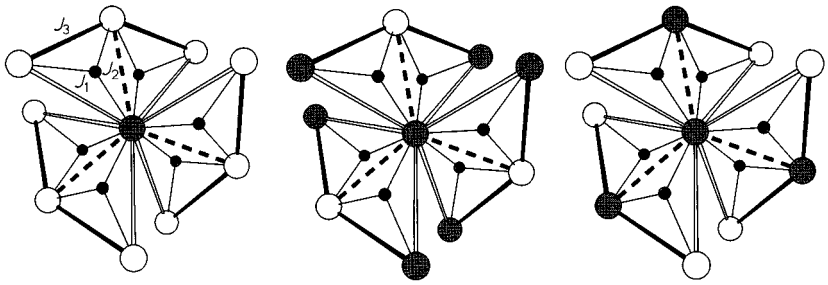

Figure 14. Schematic presentation of possible spin ground states for the M_{10} core of **2**, **4** and **7**. The filled circles represent Ni sites with spin in one direction, while the open circles represent Ni sites with spin in the opposite direction.

For **2**, the largest exchange is J_1, which is antiferromagnetic, and aligns the spin on the central Ni atom anti-parallel with the spin on the nickel atoms at the vertices of the trigonal prism. J_2 and J_3 are both ferromagnetic, but J_3 is the larger therefore the spin on the nickel centres capping the rectangular faces are aligned parallel with the spins at the vertices and anti-parallel with the spin on the central nickel. The result is that the spins on the peripheral nine nickel atoms are aligned anti-parallel with the spin on the central metal, giving a net $S=8$ ground state. For **4** the largest exchange (J_2) couples the spin of the central nickel anti-parallel with spin on the capping nickel centres. J_3 and J_1 are both ferromagnetic, but as J_1 is larger it couples the spin on the vertex nickel atoms parallel with the central metal spin. Therefore in **4** we have the spin on seven nickel centres (the central and vertex sites) aligned in one direction and the spin on three further nickel centres (the capping sites) opposed to these spins, giving an $S=4$ ground state. Finally, for **7** all the exchanges are antiferromagnetic, with the largest J_1, which aligns the spin at the centre anti-parallel with the spin at the vertices. Here J_3 is more anti-ferromagnetic than J_2, so the spin of the capping nickel centres align anti-parallel with the spins at the vertices rather than anti-parallel with the spin at the central nickel atom. The result is six nickel centres aligned in one direction (the nickel atoms at the vertices of the trigonal prism), with

0947-6539/00/0605-0894 $ 17.50+.50/0 *Chem. Eur. J.* **2000**, *6*, No. 5

the four remaining nickel centres opposed. The result is an $S = 2$ ground state.

The magnitude of the exchange parameters seems sensible for **2** and **7**, but high for **4**. Our model assumes a metal core with D_3 symmetry, and clearly for **4** the upper and lower faces of the trigonal prism are inequivalent so the symmetry could be no higher than C_3. A model containing a further three exchange parameters would give a better fit, and may lead to smaller J terms than those derived using the model described above. However we feel that the over-parameterisation this would involve, and the likely correlation between all J terms would not make this model any more satisfactory.

To remove ambiguity in the interpretation of the magnetism, further complimentary studies will be necessary. Spectroscopic techniques—in particular inelastic neutron scattering—may allow us to derive J values directly. We hope to pursue these studies in the immediate future. Our results also suggest that for structures of this complexity, understanding the relationships between structure and magnetic ground states is still impossible. However, whether our exact interpretation of how a ground state is arrived at is correct or incorrect, the important result is a direct experimental observation, and that is the maxima in the $\chi_m T/T$ plot, which implies specific values for the spin ground state of the molecule.

Experimental Section

Preparation of compounds: All reagents, metal salts and ligands were used as obtained from Aldrich. Sodium salts of pyridone ligands were obtained by deprotonation of the ligand in MeOH using Na(OMe) followed by evaporation to dryness. Analytical data were obtained on a Perkin Elmer 2400 Elemental Analyser by the University of Edinburgh Microanalytical Service and are given in Table 1.

$[Ni_{12}(OH)_6(mhp)_{12}(O_2CCH_2Cl)_6]$ (2): Hydrated nickel chloride (1.00 g, 4.21 mmol), Na(mhp) (1.104 g, 8.42 mmol) and $Na(O_2CCH_2Cl)$ (0.981 g, 8.42 mmol) were added to MeOH (30 mL), and the solution stirred for 24 h before being filtered and evaporated to dryness under reduced pressure. The solid produced was dried under vacuum overnight, then extracted with MeCN (20 mL) to give a green solution which was filtered, and from which green crystals of **2** grew in 50% yield after three days.

$[Ni_{11}(OH)_6(chp)_9(O_2CPh)_6(EtOH)_3][Ni(chp)_3]$ (where chp = 6-chloro-2-pyridonate) (3): Hydrated nickel chloride (1.00 g, 4.21 mmol), Na(chp) (1.276 g, 8.42 mmol) and $Na(O_2CPh)$ (1.212 g, 8.42 mmol) were added to EtOH (50 mL) and the solution stirred for 24 h before being filtered and evaporated to dryness under reduced pressure. The resulting solid was dried under vacuum overnight, then extracted with CH_2Cl_2 (25 mL) to give a green solution which was filtered, and from which green crystals of **3** grew in 15% yield after four days.

$[Ni_{11}(OH)_6(mhp)_9(O_2CMe)_6(H_2O)_3]_2[CO_3]$ (4): Hydrated nickel acetate (1.00 g, 4.02 mmol) and Na(mhp) were added to THF (50 mL) and the solution stirred for 24 h before being filtered and evaporated to dryness under reduced pressure. The resulting solid was dried under vacuum overnight. Hmhp (0.877 g, 8.04 mmol) was then added to the solid, and the mixture heated to 160 °C under N_2 for 2 h. The resulting paste was extracted with CH_2Cl_2 (30 mL), giving a green solution which was filtered, and from which green crystals of **4** grew in 11% yield after one week.

$[Ni_{11}(OH)_6(mhp)_9(O_2CMe)_7(Hmhp)_2]$ (5): Synthesis as for **4** except that the first stage involve MeOH in place of THF. Yield: 8% after one week.

$[Ni_{10}(OH)_6(mhp)_{6.5}(O_2CCHMe_2)_{6.5}(Hmhp)_3Cl(H_2O)]$ (6): Synthesis as for **2**, using $Na(O_2CCHMe_2)$ in place of $Na(O_2CCH_2Cl)$. Yield: 21% after one week.

$[Ni_{10}(OH)_6(chp)_6(O_2CCHPh_2)_6(Cl)_2(Hchp)(H_2O)_2(MeOH)]$ (7): Synthesis as for **2**, using $Na(O_2CCHPh_2)$ in place of $Na(O_2CCH_2Cl)$, and Na(chp) in place of Na(mhp). Yield: 27% after one week.

$[Co_{10}(OH)_6(mhp)_6(O_2CPh)_7(Hmhp)_3Cl(MeCN)]$ (8): Synthesis as for **2**, using $CoCl_2 \cdot 6H_2O$ in place of $NiCl_2 \cdot 6H_2O$, and $Na(O_2CPh)$ in place of $Na(O_2CCH_2Cl)$. Yield of pink crystals: 21% after four days.

$[Co_{10}(OH)_6(mhp)_6(O_2CCMe_3)_7Cl(MeCN)_3(Hmhp)]$ (9): Synthesis as for **2**, using $Na(O_2CCMe_3)$ in place of $Na(O_2CCH_2Cl)$. Yield of pink crystals: 23% after two days.

$[Ni_{10}(OH)_4(mhp)_{10}(O_2CCMe_3)_6(MeOH)_2]$ (10): Synthesis as for **2**, using $Na(O_2CCMe_3)$ in place of $Na(O_2CCH_2Cl)$. Yield: 45% after three days.

$[Ni_{10}(OH)_4(mhp)_{10}(O_2CCMe_3)_6(H_2O)_2]$ (11): Synthesis as for **2**, using $Na(O_2CCMe_3)$ in place of $Na(O_2CCH_2Cl)$ and crystallisation from 1:1 MeCN/EtOAc. Yield: 18% after 10 weeks.

$[Co_{10}(OH)_4(chp)_{10}(O_2CCMe_3)_6(H_2O)_2]$ (12): $CoCl_2 \cdot 6H_2O$ (1 g, 4.2 mmol), $Na(O_2CCMe_3)$ (0.522g, 4.2 mmol) and Na(chp) (1.272 g, 8.4 mmol) were mixed together in MeOH (50 mL) and stirred for 24 h. The solvent was then removed under reduced pressure and the resulting purple powder dried under vacuum for 6 h. Disodium rhodizonate (0.075 g, 0.35 mmol) was dissolved in 1:1 H_2O:MeOH (50 mL) and the purple powder was extracted with this solution. The resulting solution was stirred for 24 h before solvent was removed under reduced pressure. The powder was dried in vacuum for 4 h before being extracted with EtOH. Purple crystals of **12** formed over a period of two months. Yield: 21%.

Crystallography: Crystal data and data collection and refinement parameters for compounds **2**–**12** are given in Table 2, selected bond lengths and angles in Tables 3, 4, 5 and 6.

Data collection and processing: Data for **2**–**11** were collected on a Stoë Stadi-4 four-circle diffractometer equipped with an Oxford Cryosystems low-temperature device,[16] using graphite-monochromated $Cu_{K\alpha}$ radiation for **3**, **6**, **10** and **11**, and $Mo_{K\alpha}$ radiation for **2**, **4**, **5**, **7**–**9**; ω-θ scans for **2** and **11**, ω scans for **3**–**7**, **9** and **10**. The learnt-profile method[17] was used for **3**, **6** and **8**. Data were corrected for Lorentz and polarisation factors. Semi-empirical absorption corrections based on azimuthal measurements[18] were applied to data for all structures except **4**. Data for **12** were collected on an Enraf Nonius Kappa CCD area detector using a rotating anode operating at 50 KV, 50 mA using $Mo_{K\alpha}$ radiation. Data collection and processing used the programs Collect[19], DENZO[20] and maXus[21]. An empirical absorption correction was applied using SORTAV.[22]

Structure analysis and refinement: All structures were solved by direct methods using SHELXS-86[23] (**2**, **4**, **5** and **10**) or SIR92[24] (**3**, **6**, **8**, **9** and **12**) or by the heavy-atom method using DIRDIF[25] (**7** and **11**) and completed by iterative cycles of difference Fourier syntheses and full-matrix least-squares refinement. All full-weight non-H atoms were refined anisotropically in structures **2**, **3**, **4**, **5**, **8**, **9**, **10** and **11**, while only Ni, O and Cl atoms were so refined in **6** and **7**. In **12** all non-H atoms within the cage were refined anisotropically except for disordered carbon atoms within two O_2CCMe_3 groups. In **2** two of the six chloroacetate ligands show rotational disorder about the Cl-C-C vector. They were refined with the Cl centre split over three sites, with the site occupancies allowed to refine but summing to one complete chlorine atom. Chemically equivalent distances were restrained to be equal. In **6**–**8** all chemically equivalent ligands were restrained to have similar geometries. In **8** global rigid body restraints and similarity restraints were applied to the mhp rings. In **6** one coordination site on Ni3 is occupied 50:50 by H_2O:mhp, while on Ni10 one site is 50:50 occupied by O_2CCHMe_2:H_2O. Similar disorder is found in **7** where one site on Ni2 is occupied 50:50 by MeOH:Hchp, and in **8** where neighbouring sites on Co5 and Co8 are 50:50 occupied by Cl:mhp. In **7** one phenyl ring of a O_2CCHPh_2 ligand is disordered over two equal-weight orientations. In **8** one Hmhp ligand attached to Co2 has disordered over two equal-weight orientations, with a common pivot O atom. In **6** the *i*Pr and in **9**–**11** the *t*Bu groups of the carboxylate ligands show rotational disorder. In **10**, **11** and **12** the O_2CCMe_3 ligands were restrained to be geometrically similar; the *t*Bu groups have three-fold symmetry. In **8** global thermal parameter similarity restraints were applied to the light atoms. Disordered solvent fragments were found in structures **2**–**5**, **7**, **10**, **11** and **12**. In **2** and **5** diffuse lattice solvent regions comprising 83 and 55e/cell, respectively, were treated in the manner described by van der Sluis and Speck.[26] In **5** residual density remains in the region of the CH_2Cl_2 of solvation. In **3** one Et_2O molecules of solvation lies disordered about a crystallographic three-fold axis; compo-

site scattering factors were used for overlapping sites. In **12** one MeOH molecule was found disordered over three sites, and the C–O distance was restrained to 1.4 Å. In all structures full-weight H atoms attached to C atoms were included in idealised positions, allowed to ride on their parent C atoms [C–H 0.93 Å], and assigned isotropic thermal parameters [$U(H) = 1.2\,U_{eq}$] for ring H-atoms; $U(H) = 1.5\,U_{eq}$ for methyl H atoms]. Full-weight H atoms attached to O atoms were included in positions to maximise H-bonding interactions, and assigned isotropic thermal parameters [$U(H) = 1.5\,U_{eq}(O)$]. Partial weight H atoms were not included in refinements. All refinements were against F^2 and used SHELXL-93[27] or SHELXL-97.[13]

Crystallographic data (excluding structure factors) for the structures reported in this paper have been deposited with the Cambridge Crystallographic Data Centre as supplementary publication no. CCDC-132601 to 132611. Copies of the data can be obtained free of charge on application to CCDC, 12 Union Road, Cambridge CB2 1EZ, UK (fax: (+44) 1223-336-033; e-mail: deposit@ccdc.cam.ac.uk).

Magnetic measurements: Magnetic susceptibility measurements were performed either on a DSM 5 magnetometer equipped with a Bruker BE-15 electromagnet and an Oxford Instruments CF1200S continuous-flow cryostat, or on an SHE superconducting SQUID susceptometer. Data were corrected for magnetisation of the sample holder and for diamagnetic contributions with Pascal's constants.

Acknowledgements

We thank the EPSRC (UK) for funding for a diffractometer and for studentships (for E. K. B, A. G. and S. G. H.). We also than NATO and COST Action 518 for support of the collaboration between Edinburgh and Florence.

[1] a) R. Sessoli, H.-L. Tsai, A. R. Schake, S. Wang, J. B. Vincent, K. Folting, D. Gatteschi, G. Christou, D. N. Hendrickson, *J. Am. Chem. Soc*. **1993**, *115*, 1804 – 1816; b) R. Sessoli, D. Gatteschi, A. Caneschi, M. A. Novak, *Nature* **1993**, *365*, 141 – 142; c) H. J. Eppley, H. -L. Tsai, N. de Vries, K. Folting, G. Christou, D. N. Hendrickson, *J. Am. Chem. Soc*. **1995**, *117*, 301 – 317; d) C. Sangregorio, T. Ohm, C. Paulsen, R. Sessoli, D. Gatteschi, *Phys. Rev. Lett*. **1997**, *78*, 4645 – 4648; e) M. W. Wemple, D. M. Adams, K. S. Hagen, K. Folting, D. N. Hendrickson, G. Christou, *J. Chem. Soc. Chem. Commun.* **1995**, 1591 – 1593; f) Z. Sun, C. M. Grant, S. L. Castro, D. N. Hendrickson, G. Christou, *Chem. Commun.* **1998**, 721 – 722; g) E. K. Brechin, J. Yoo, M. Nakano, J. C. Huffman, D. N. Hendrickson, G. Christou, *Chem. Commun.* **1999**, 783 – 784.

[2] a) J. Friedman, M. Sarachik, J. Tejada, R. Ziolo, *Phys. Rev. Lett.* **1996**, *76*, 3830 – 3833; b) L. Thomas, F. Lionti, R. Ballou, D. Gatteschi, R. Sessoli, B. Barbara, *Nature* **1996**, *383*, 145 – 146.

[3] Z. M. Sun, D. Ruiz, E. Rumberger, C. D. Incarvito, K. Folting, A. L. Rheingold, G. Christou, D. N. Hendrickson, *Inorg. Chem.* **1998**, *37*, 4758 – 4759.

[4] a) S. Parsons, R. E. P. Winpenny, *Acc. Chem. Res.* **1997**, *30*, 89 – 98; b) R. E. P. Winpenny, *Comm. Inorg. Chem.* **1999**, *20*, 233 – 262.

[5] A. J. Blake, C. M. Grant, S. Parsons, J. M. Rawson, R. E. P. Winpenny, *J. Chem. Soc. Chem. Commun.* **1994**, 2363 – 2364.

[6] E. K. Brechin, S. G. Harris, A. Harrison, S. Parsons, A. G. Whittaker, R. E. P. Winpenny, *Chem. Commun.* **1997**, 653 – 654.

[7] W. Clegg, C. D. Garner, M. H. Al-Samman, *Inorg. Chem.* **1983**, *22*, 1534 – 1538.

[8] A. J. Blake, E. K. Brechin, A. Codron, R. O. Gould, C. M. Grant, S. Parsons, J. M. Rawson, R. E. P. Winpenny, *J. Chem. Soc. Chem. Commun.* **1995**, 1983 – 1985.

[9] E. K. Brechin, S. Parsons, R. E. P. Winpenny, *Dalton Trans.* **1996**, 3745 – 3746.

[10] E. K. Brechin, S. G. Harris, S. Parsons, R. E. P. Winpenny, *Chem. Commun.* **1996**, 1439 – 1440.

[11] G. A. Jeffrey, *An Introduction to Hydrogen Bonding*, Oxford University Press, New York, **1997**, p. 62.

[12] A. Graham. S. Parsons, A. M. Seddon, R. E. P. Winpenny, unpublished results.

[13] G. M. Sheldrick, University of Göttingen, **1997**.

[14] K. K. Nanda, L. K. Thompson, J. N. Bridson, K. Nag, *J. Chem. Soc. Chem. Comm.* **1994**, 1337 – 1338.

[15] M. A. Halcrow, J.-S. Sun, J. C. Huffman, G. Christou, *Inorg. Chem.* **1995**, *34*, 4167 – 4177.

[16] J. Cosier, A. M. Glazer, *J. Appl. Crystallogr.* **1986**, *19*, 105 – 107.

[17] W. Clegg, *Acta Crystallogr. Sect. A* **1981**, *37*, 22 – 28.

[18] A. C. T. North, D. C. Phillips, F. S. Mathews, *Acta Crystallogr. Sect. A* **1968**, *24*, 351 – 359.

[19] "Collect" data collection software, Nonius B. V. **1998**.

[20] Z. Otwinowski, W. Minor in *Methods in Enzymology*, *Vol. 276: Macromolecular Crystallography*, *part A* (Eds.: C. W. Carter, Jr., R. M. Sweet), Academic Press, Dordrecht, **1997**, pp. 307 – 326.

[21] S. Mackay, C. J. Gilmore, C. Edwards, M. Tremayne, N. Stuart, K. Shankland, University of Glasgow, UK, Nonius B. V., Delft, The Netherlands and MacScience Co. Ltd., Yokohama, Japan, **1998**.

[22] R. H. Blessing, *Acta Crystallogr. Sect. A* **1995**, *51*, 33 – 39.

[23] G. M. Sheldrick, *Acta Crystallogr. Sect. A* **1990**, *46*, 467 – 473.

[24] A. Altomare, G. Cascarano, C. Giacovazzo, A. Guagliardi, *J. Appl. Cryst.* **1993**, *26*, 343 – 350.

[25] P. T. Beurskens, G. Beurskens, W. P. Bosman, R. de Gelder, S. Garcia-Granda, R. O. Gould, R. Israel, J. M. M. Smits, DIRDIF-96 program system, University Crystallography Laboratory, University of Nijmegen, **1996**.

[26] P. van der Sluis, A. L. Spek, *Acta Crystallogr. Sect. A* **1990**, *46*, 194 – 201.

[27] G. M. Sheldrick, SHELXL-93, program for crystal structure refinement, University of Göttingen, **1993**.

Received: July 27, 1999 [F 1939]

  0947-6539/00/0605-0896 $ 17.50+.50/0